Supporting Information

Unveiling Li-/Sr-induced reinforced transition metal-oxygen in P2-type layered oxide cathode for highly stable sodium-ion batteries

Jiashuo Wang[#], Linkai Guo[#], Chang Liu, Kun Li, Wenchang Wang, Yurong Ren, Huilong Dong[*], Zhidong Chen[*], Changhai Liu[*]

Jiashuo Wang, Linkai Guo, Chang Liu, Kun Li, Yurong Ren, Changhai Liu
School of Materials Science and Engineering, CNPC-CZU Innovation Alliance, Changzhou University, Changzhou, 213164, Jiangsu, China
E-mail: liuch@cczu.edu.cn
Wenchang Wang, Zhidong Chen
bSchool of Petrochemical Engineering, Changzhou University, Changzhou, Jiangsu, 213164, China
E-mail: zdchen@cczu.edu.cn
Huilong Dong
cSchool of Materials Engineering, Suzhou University of Technology, Changshu, Jiangsu 215500, China.
E-mail: hldong@szut.edu.cn

Experimental section

materials

Anhydrous sodium carbonate (Na_2CO_3, AR), nickel(II) oxide (NiO, ≥99.9 %), manganese dioxide (MnO_2, ≥99.9 %), lithium carbonate (Li_2CO_3, AR), strontium carbonate ($SrCO_3$, AR) , anhydrous ethanol (C_2H_5OH, ≥99.7 %), Polyvinylidene Fluoride(PVDF), conductive carbon black material(Super P), N-Methylpyrrolidone(NMP, ≥99.9 %).

synthetic method

The preparation method of P2-$Na_{0.67}Ni_{0.33}Mn_{0.67}O_2$ is as follows: Initially, anhydrous sodium carbonate, nickel(II) oxide, and manganese dioxide were weighed in stoichiometric proportions, added into a ball mill jar, followed by dropwise addition of 2 mL anhydrous ethanol. The mixture was placed in a planetary ball mill and wet-milled at 450 r/min for 12 h. Subsequently, the obtained mixed powder was dried in a blast drying oven. The dried powder was transferred to a muffle furnace for sintering in air atmosphere: first, it was heated to 500 ℃ at a heating rate of 2 ℃/min and held for 6 h; then heated to 950 ℃ at a heating rate of 5 ℃/min and held for 15 h; finally, it was cooled naturally to room temperature to obtain P2-$Na_{0.67}Ni_{0.33}Mn_{0.67}O_2$.

The preparation method of P2-$Na_{0.67}Ni_{0.31}Li_{0.02}Mn_{0.67}O_2$ is as follows: Initially, anhydrous sodium carbonate, nickel(II) oxide, manganese dioxide, and lithium carbonate were weighed in stoichiometric proportions, added into a ball mill jar, followed by dropwise addition of 2 mL anhydrous ethanol. The mixture was placed in a planetary ball mill and wet-milled at 450 r/min for 12 h. Subsequently, the obtained mixed powder was dried in a blast drying oven. The dried powder was transferred to a muffle furnace for sintering in air atmosphere: first, it was heated to 500 ℃ at a heating rate of 2 ℃/min and held for 6 h; then heated to 950 ℃ at a heating rate of 5 ℃/min and held for 15 h; finally, it was cooled naturally to room temperature to obtain P2-$Na_{0.67}Ni_{0.31}Li_{0.02}Mn_{0.67}O_2$.

The preparation method of P2-$Na_{0.65}Sr_{0.02}Ni_{0.33}Mn_{0.67}O_2$ is as follows: Initially, anhydrous sodium carbonate, nickel(II) oxide, manganese dioxide, and strontium carbonate were weighed in stoichiometric proportions, added into a ball mill jar,

followed by dropwise addition of 2 mL anhydrous ethanol. The mixture was placed in a planetary ball mill and wet-milled at 450 r/min for 12 h. Subsequently, the obtained mixed powder was dried in a blast drying oven. The dried powder was transferred to a muffle furnace for sintering in air atmosphere: first, it was heated to 500 ℃ at a heating rate of 2 ℃/min and held for 6 h; then heated to 950 ℃ at a heating rate of 5 ℃/min and held for 15 h; finally, it was cooled naturally to room temperature to obtain P2-$Na_{0.65}Sr_{0.02}Ni_{0.33}Mn_{0.67}O_2$.

P2-$Na_{0.66}Sr_{0.01}Ni_{0.32}Li_{0.01}Mn_{0.67}O_2$ was prepared via a solid-state sintering method, with the specific procedure as follows: Initially, anhydrous sodium carbonate, nickel(II) oxide, manganese dioxide, strontium carbonate, and lithium carbonate were weighed in stoichiometric proportions, added into a ball mill jar, followed by dropwise addition of 2 mL anhydrous ethanol. The mixture was placed in a planetary ball mill and wet-milled at 450 r/min for 12 h. Subsequently, the obtained mixed powder was dried in a blast drying oven. The dried powder was transferred to a muffle furnace for sintering in air atmosphere: first, it was heated to 500 ℃ at a heating rate of 2 ℃/min and held for 6 h; then heated to 950 ℃ at a heating rate of 5 ℃/min and held for 15 h; finally, it was cooled naturally to room temperature to obtain P2-$Na_{0.66}Sr_{0.01}Ni_{0.32}Li_{0.01}Mn_{0.67}O_2$.

Characterization

The specific procedures for cathode preparation and coin cell (half-cell/full-cell) assembly are as follows: The active material (P2-$Na_{0.66}Sr_{0.01}Ni_{0.32}Li_{0.01}Mn_{0.67}O_2$), Super P conductive agent, and PVDF binder were weighed at a mass ratio of 8:1:1, added into N-methylpyrrolidone (NMP) solvent for dispersion, and uniformly mixed into a slurry by stirring; the slurry was coated onto aluminum foil current collector using a doctor blade with a height of 200 μm, then the coated aluminum foil was dried in a vacuum drying oven at 120 ℃ for 12 h, the dried electrode sheet was cut into circular cathode sheets with a diameter of 12 mm, whose active material mass loading was controlled within the range of 1.5-2.5 mg/cm², and the cathode sheets were transferred to a glove box filled with high-purity Ar for standby. Coin cells were assembled in an MBRAUN glove box under high-purity N_2 protection (both H_2O and O_2 contents < 0.1 ppm); for half-cell assembly, the electrolyte was 1 M $NaPF_6$ in ethylene methyl carbonate (EMC): propylene carbonate (PC) (1:1, v/v) with 4% fluoroethylene carbonate (FEC) as additive, Whatman GF/D glass fiber membrane was used as the separator, and metallic

sodium sheet served as the counter electrode; the full-cell assembly procedure was the same as that of the half-cell, with Type-2 hard carbon as the anode, the above-prepared P2-$Na_{0.66}Sr_{0.01}Ni_{0.32}Li_{0.01}Mn_{0.67}O_2$ cathode sheet as the cathode, and the separator and electrolyte specifications consistent with those of the half-cell.

The assembled half-cells were allowed to stand at room temperature for 24 h before electrochemical measurements, with a test voltage window of 2-4.2 V. Specifically, the rate performance test, cycle performance test, galvanostatic intermittent titration technique (GITT) test, and ion diffusion coefficient test were conducted on a Xinwei high-performance battery testing system (CT-4008Q-5V50mA-HWX); electrochemical impedance spectroscopy (EIS) measurements and cyclic voltammetry (CV) measurements were performed on a DH700C electrochemical workstation. The in-situ EIS test conditions were: low frequency 0.01 Hz, high frequency 100000 Hz, and amplitude 5 mV; the CV test conditions were: vertex voltages 2 V and 4.2 V, single scan rate 0.2 mV/s, and scan rates for multi-rate tests were 0.2 mV/s, 0.4 mV/s, 0.6 mV/s, 0.8 mV/s, 1 mV/s respectively. The relaxation time distribution of the battery was obtained by fitting the in-situ impedance data using Matlab software.

The surface morphology and elemental distribution of the samples were characterized by scanning electron microscopy (SEM, JSM-6360LA, Japan) and energy dispersive spectroscopy (EDS, EX54175JMU). X-ray photoelectron spectroscopy (XPS, Thermo Scientific) was used to analyze the valence states of different elements in the electrode materials, with Al Kα radiation as the excitation source. The surface microstructure of the samples was examined by high-resolution transmission electron microscopy (HRTEM, JEOL 2100). The crystal structure changes of the batteries during charge-discharge processes were tested by X-ray diffractometer (XRD, D8 Advance) with Cu Kα radiation. The XRD data were refined by fitting with Fullprof software, and the used Crystallographic Information File (CIF) card number was 4002260.

Calculations details

The density functional theory (DFT) calculations were performed by the Vienna ab initio simulation package (VASP). The ground state ion-electron wave-functions

were described by the projected augmented wave (PAW) method, with a kinetic cutoff energy of 400 eV. The electron exchange and correlation was expressed by proposed by Perdew-Burke-Ernzerhof functional within the framework of generalized gradient approximation (GGA-PBE). The convergence criterion for total energy and residual force were set as 10^{-5} eV and 0.02 eV/Å, respectively. The hexagonal lattice of NNM (symmetry group: $P6_3/mcm$) was taken as the initial unit cell, which is composed of layered $NiMn_2O_6$ backbone and the intercalated sodium cations (Na^+). After the optimization of lattice constants, we then expanded the unit cell into a $\sqrt{3} \times \sqrt{3}$ supercell, with a total composition of $Na_{12}Ni_6Mn_{12}O_{36}$. The Sr-doped NNM and Li-doped NNM were then modeled by substituting one of the cations from the original NNM supercell into Sr or Li. The Brillouin zone was sampled by gamma-centered 8 × 8 × 3 k-point meshes during lattice optimization of NNM unit cell, and 4 × 4 × 3 k-point meshes were used for structural relaxation of the doped NNM structures. The formation energy (E_f) was calculated by Equation (1)

$$E_f = \frac{1}{n}(E_{total} - \sum_{i=1}^{m} n_i \mu_i) \quad (1)$$

where the n is the total number of atoms in the calculated structure and E_{total} is the corresponding total energy, n_i is the atomic number of element i and μ_i is the corresponding chemical potential.

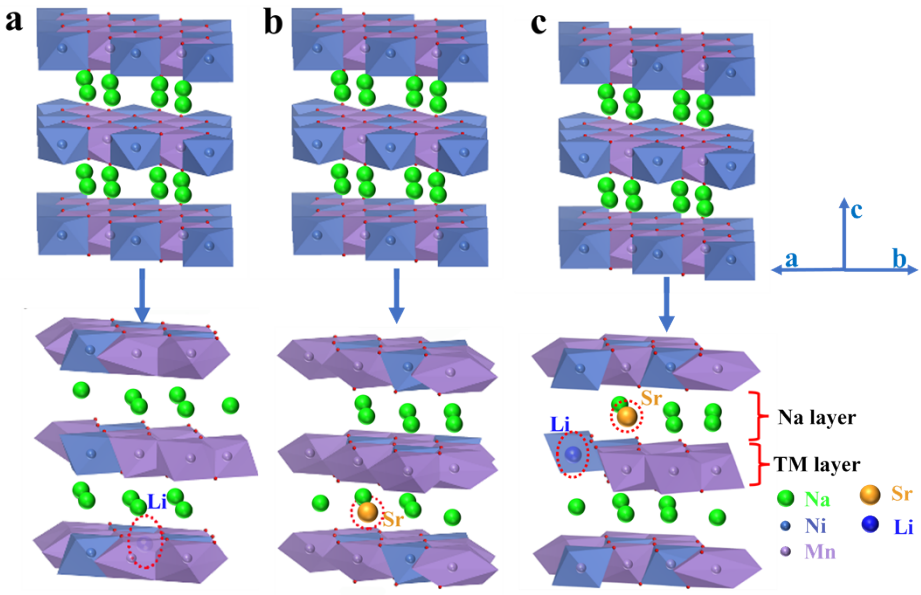

Figure S1 Schematic diagrams of the crystal structure before and after doping:(a)NNM-L;(b)NNM-S;(c)NNM-LS.

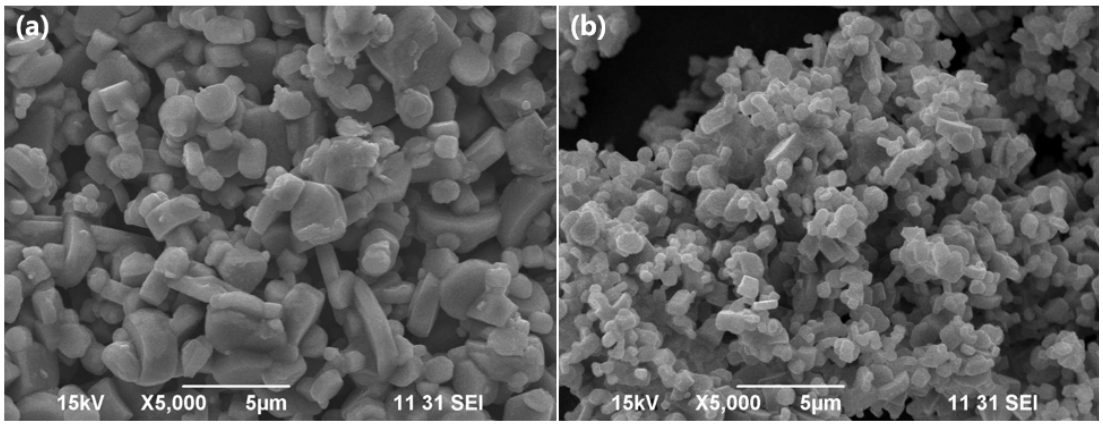

Figure S2 SEM images of (a)NNM-L;(b)NNM-S.

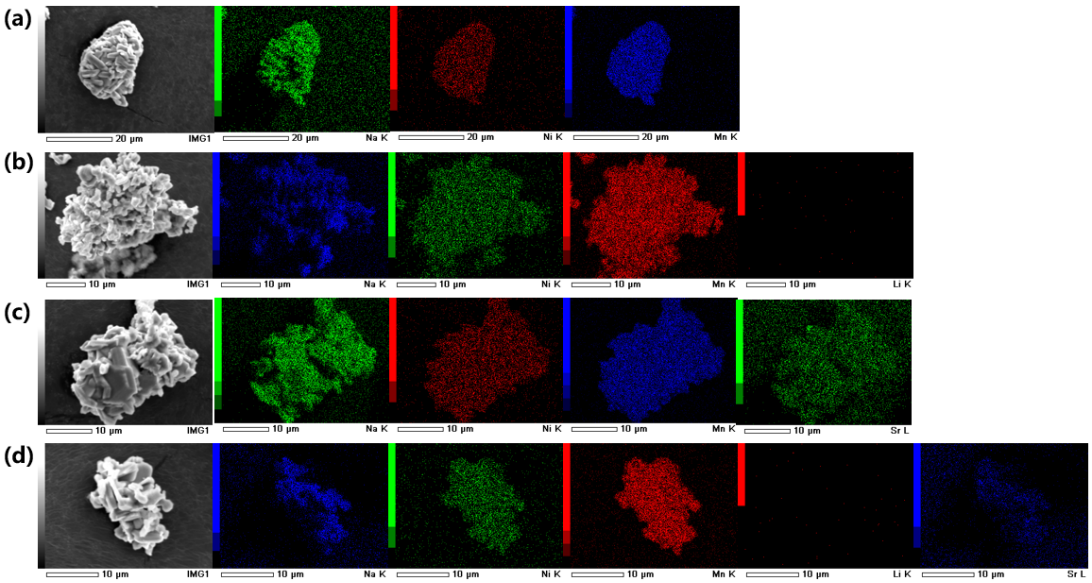

Figure S3 EDS elemental mappings of (a)NNM;(b)NNM-L;(c)NNM-S;(d)NNM-LS.

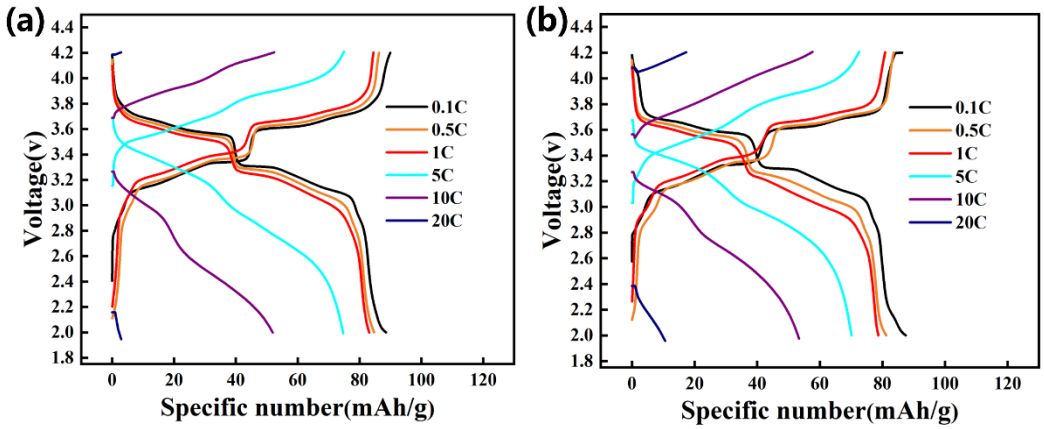

Figure S4 The first-cycle charge and discharge curves of each material at different rates:(a)NNM-L;(b)NNM-S.

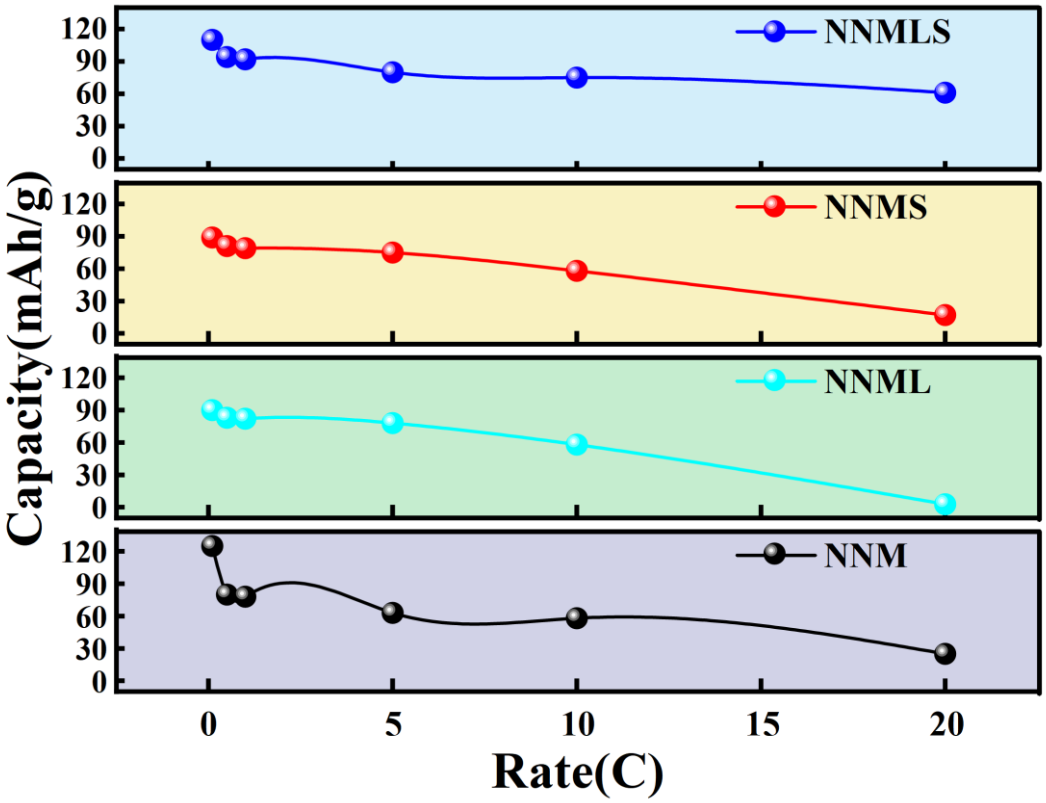

Figure S5 The capacity retention conditions of different samples at 0.1C、0.5C、1C、5C、10C、20C.

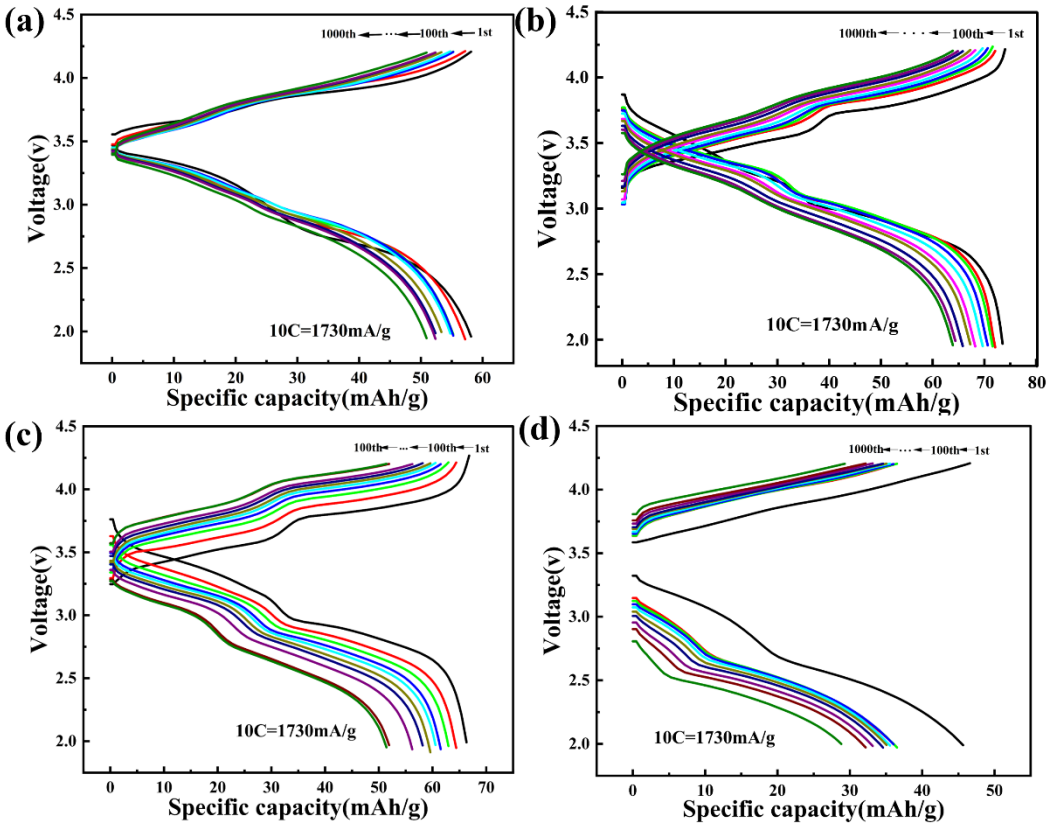

Figure S6 At a 10C rate cycle, the charge-discharge curve per 100 turns: (a)NNM; (b)NNM-LS; (c)NNM-L; (d)NNM-S.

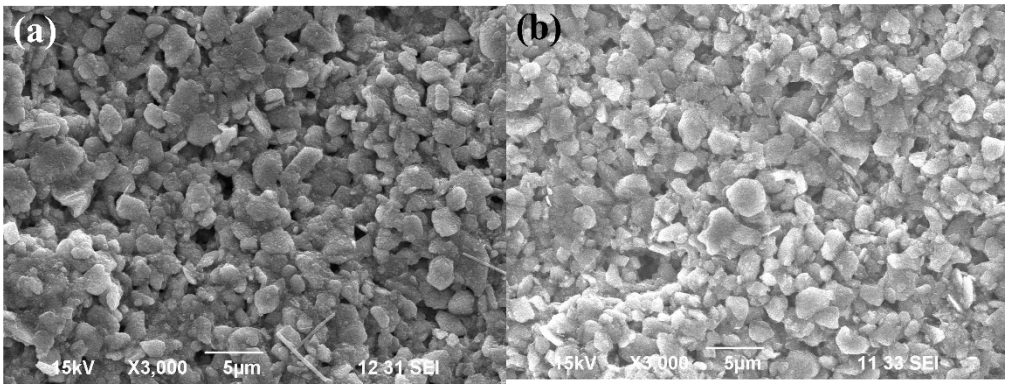

Figure S7 The SEM image of the electrode sheet after 1000 cycles at 10C:(a)NNM;(b)NNM-LS

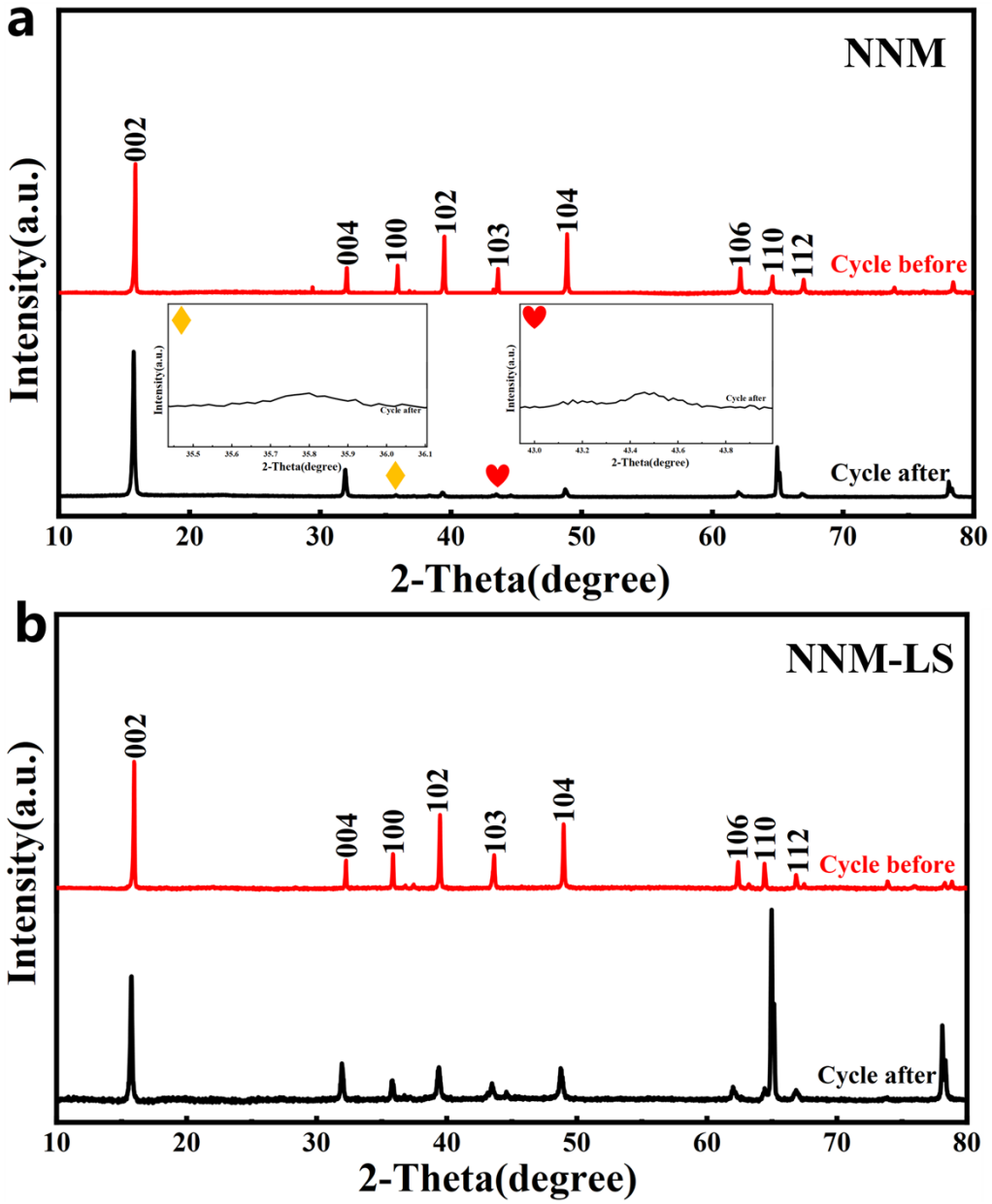

Figure S8. XRD of the cathode material of the battery before and after cycling:(a)NNM;(b)NNM-LS.

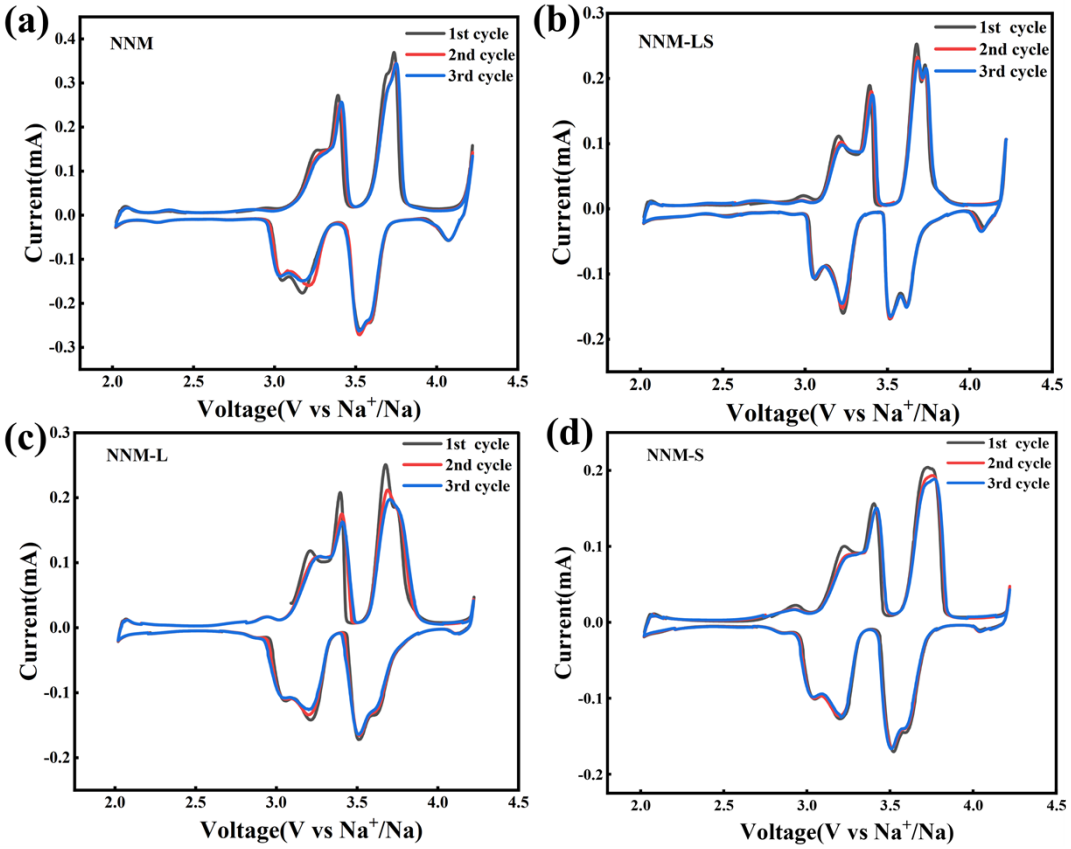

Figure S9 CV curves at 0.2 mV s^{-1} in the initial three cycles of (a)NNM;(b)NNM-LS;(c)NNM-L;(d)NNM-S.

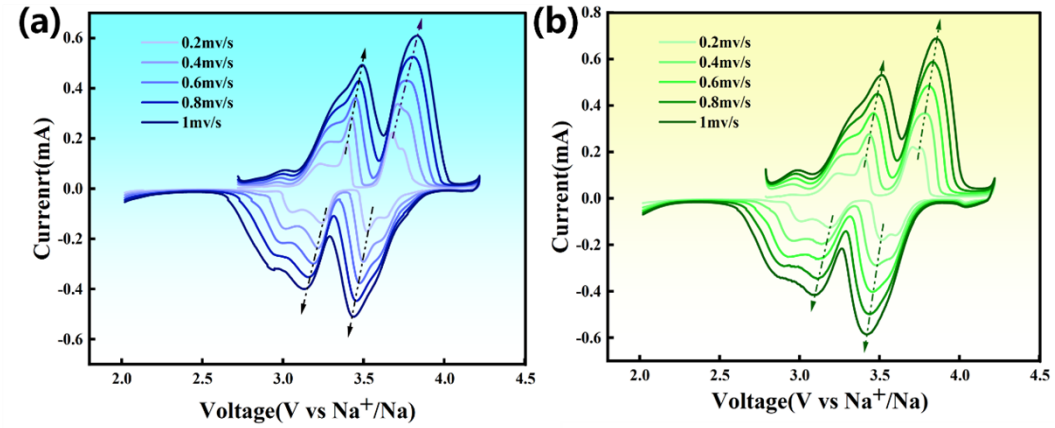

Figure S10 CV curves at different scan rates (0.2-1.0mV/S)：(a)NNM-L;(b)NNM-S.

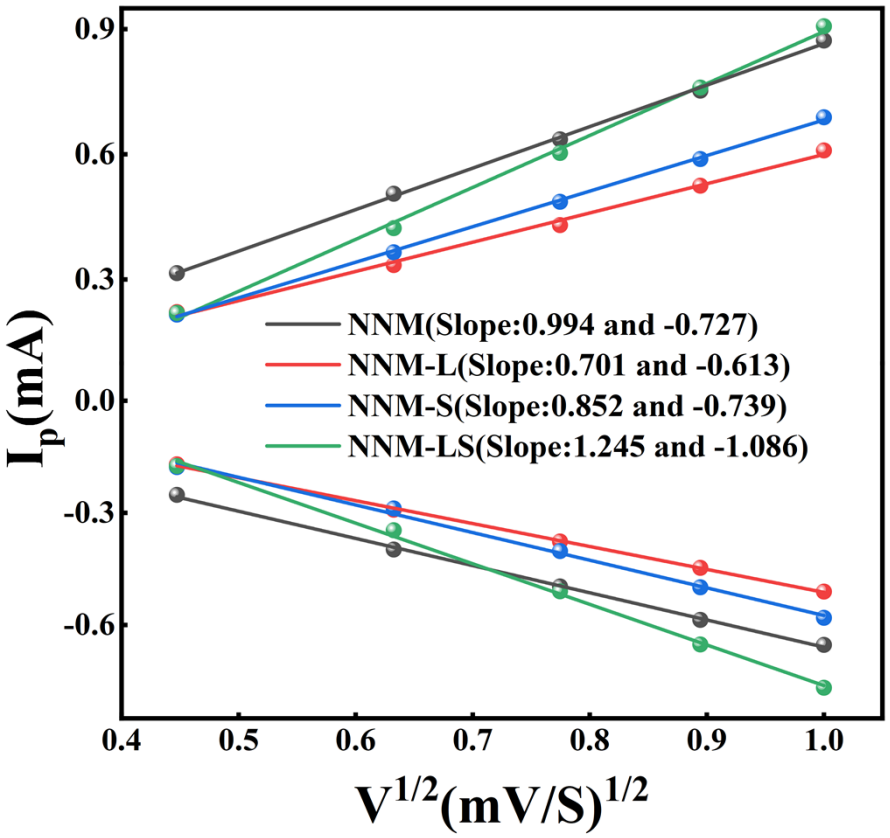

Figure S11 Linear fitting plot of the square root of the curve of the peak current (Ip) and the sweep rate ($v_{1/2}$) of the redox peak for four sample

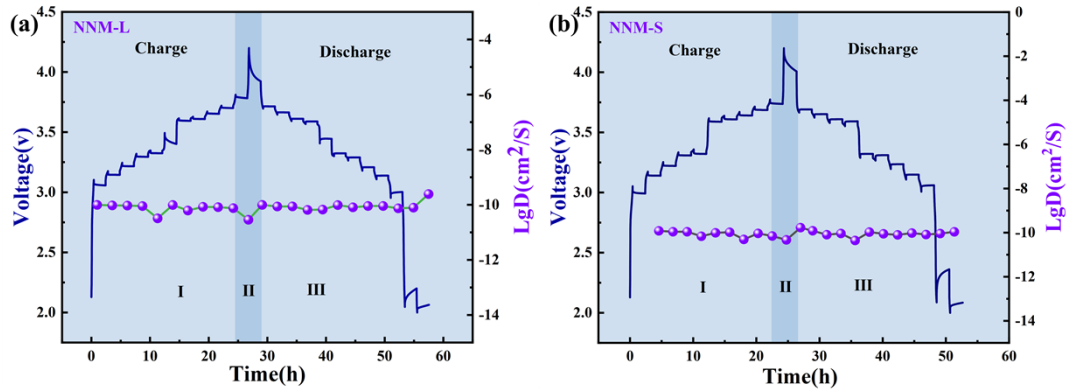

Figure S12 GITT curves and corresponding D_{Na+} values of (a)NNM-L;(b)NNM-S.

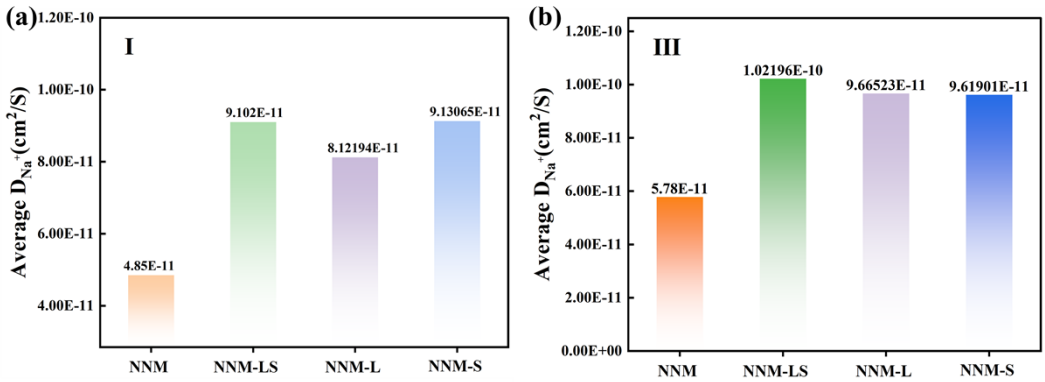

Figure 13 The average sodium ion diffusion coefficient in different regions(a)I;(b)III

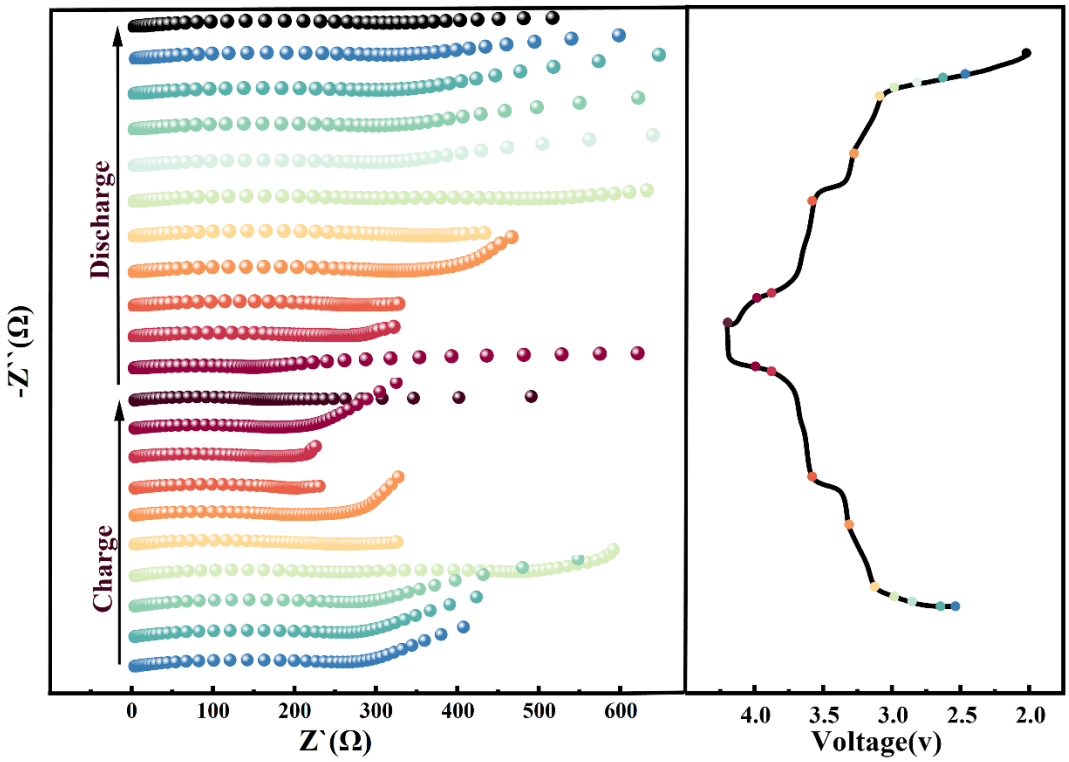

Figure S14 The impedance corresponding to different voltages on the NNM-LS charge and discharge curve

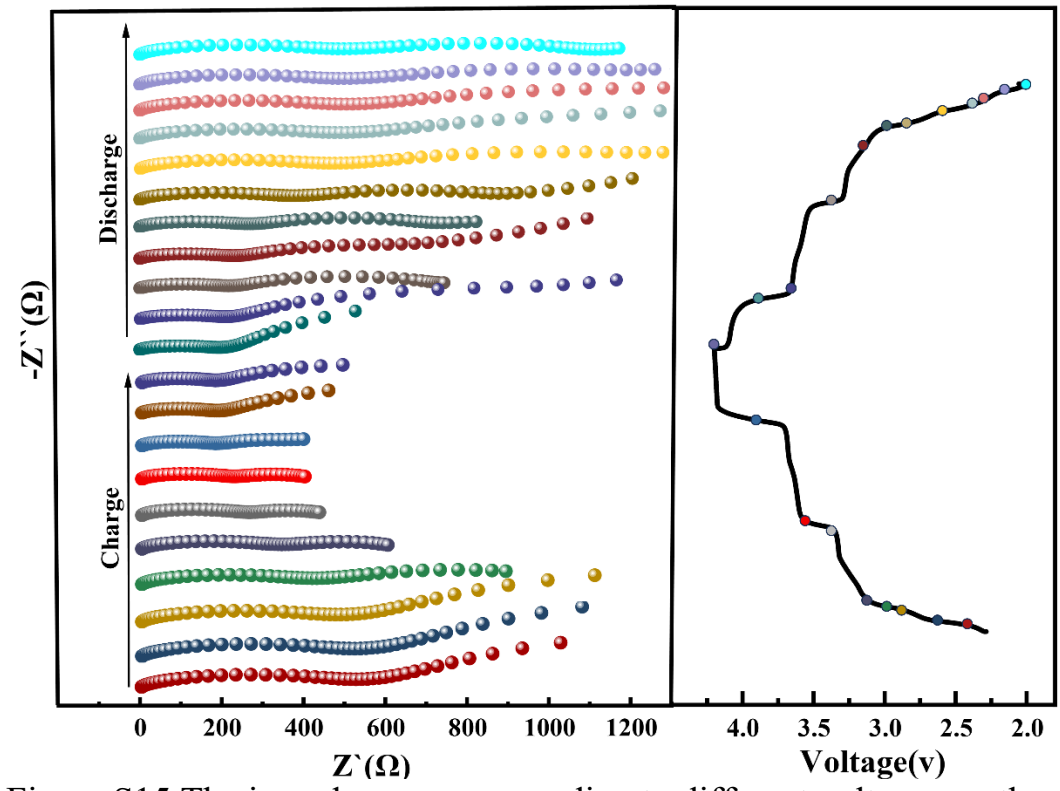

Figure S15 The impedance corresponding to different voltages on the NNM charge and discharge curve

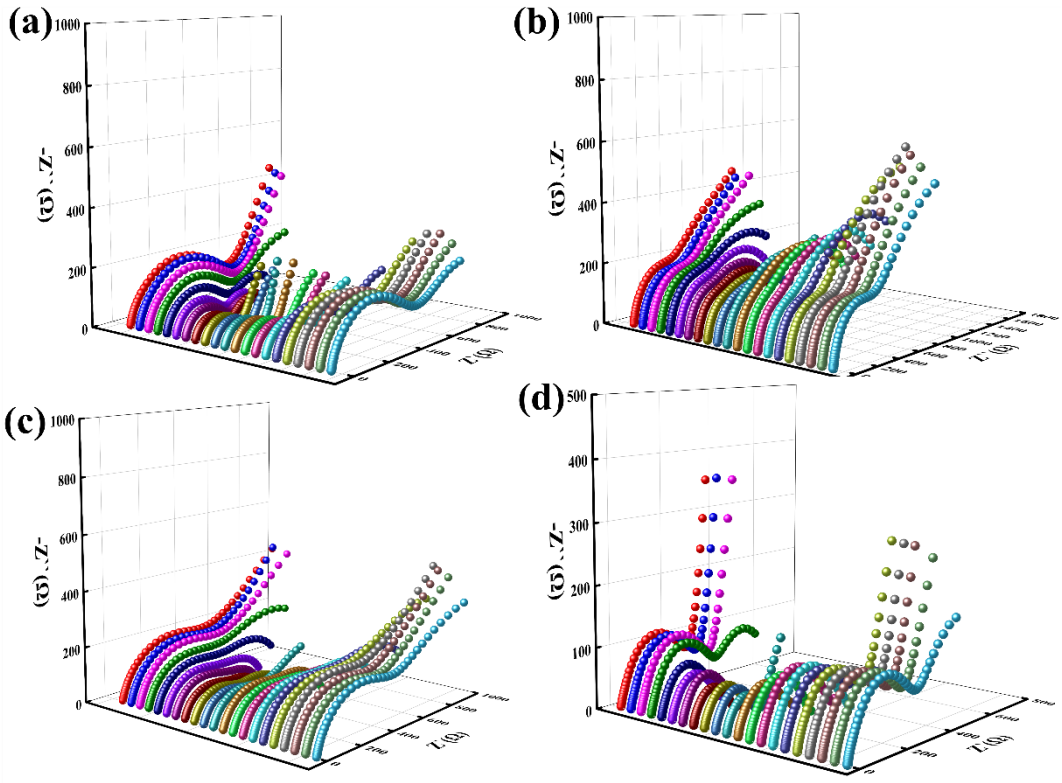

Figure S16 EIS at different voltages:(a)NNM;(b)NNM-L;(c)NNM-S;(d)NNM-LS.

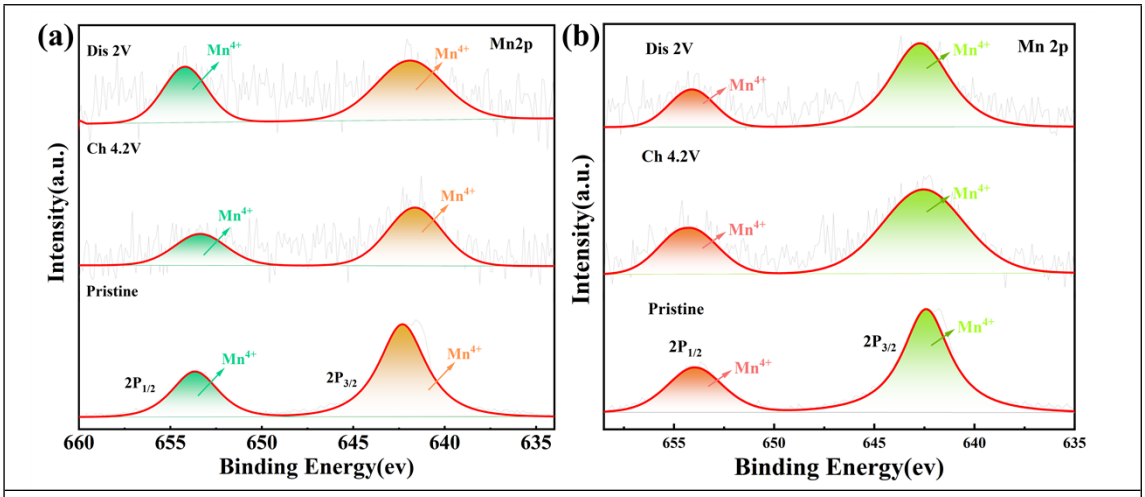

Figure S17. Ex situ X-ray photoelectron spectroscopy analysis of Mn 2p:(a)NNM-LS;(b)NNM.

Table S1.ICP-AES results of four samples

Chemical formula	Measured atomic ratio				
	Na	Ni	Mn	Li	Sr
$Na_{0.67}Ni_{0.33}Mn_{0.67}O_2$	0.6681	0.3254	0.6722	0	0
$Na_{0.67}Ni_{0.31}Li_{0.02}Mn_{0.67}O_2$	0.6651	0.3082	0.6742	0.017	0
$Na_{0.65}Sr_{0.02}Ni_{0.33}Mn_{0.67}O_2$	0.6523	0.3305	0.6735	0	0.021
$Na_{0.66}Sr_{0.01}Ni_{0.32}Li_{0.01}Mn_{0.67}O_2$	0.6608	0.3209	0.6728	0.012	0.014

Table S2 The atomic occupancy rate obtained of NNM by XRD

atom	site	x	y	z	Occ
Na_f	2b	0	0	0.25	0.25
Na_e	2d	0.67	0.33	0.25	0.42
Ni	2a	0	0	0	0.33
Mn	2a	0	0	0	0.67
O	4f	0.67	0.33	0.09	1

Table S3 The atomic occupancy rate obtained of NNM-Li by XRD

atom	site	x	y	z	Occ
Na_f	2b	0	0	0.25	0.25
Na_e	2d	0.67	0.33	0.25	0.42
Ni	2a	0	0	0	0.31
Mn	2a	0	0	0	0.67
Li	2a	0	0	0	0.02
O	4f	0.67	0.33	0.08	1

Table S4 The atomic occupancy rate obtained of NNM-Sr by XRD

atom	site	x	y	z	Occ
Na_f	2b	0	0	0.25	0.25
Na_e	2d	0.67	0.33	0.25	0.40
Ni	2a	0	0	0	0.33
Mn	2a	0	0	0	0.67
Sr	2d	0	0	0	0.02
O	4f	0.67	0.33	0.09	1

Table S5 The atomic occupancy rate obtained of NNM-LS by XRD

atom	site	x	y	z	Occ
Na_f	2b	0	0	0.25	0.25
Na_e	2d	0.67	0.33	0.25	0.41
Ni	2a	0	0	0	0.33
Mn	2a	0	0	0	0.67
Sr	2d	0	0	0	0.01
Li	2a	0	0	0	0.01
O	4f	0.67	0.33	0.09	1

Table S6.The electrochemical performance comparison between NNM-LS and other typical cathode materials reported.

Cathode material	Max rate (C)/Specific capacity(mAh/g)	capacity retention (%)/Cycle numbers(n)	Ref
NNM-LS	20C/62 mAh g^{-1}	84.1%/300	*This Work*
$K_xFe_{0.2}Mn_{0.8-y}Mg_yO_2$	10C/25 mAh g^{-1}	79.1%/200	[1]
TiO_2@$Na_{0.85}Li_{0.12}Ni_{0.22}Mn_{0.66}O_2$	2C/64.2 mAh g^{-1}	85.4%/200	[2]
$Na_{0.8}Cu_{0.2}Fe_{0.4}Mn_{0.4}O_2$	2C/30 mAh g^{-1}	69.12%/100	[3]
$Na_{0.67}Li_{0.1}(Ni_{0.33}Mn_{0.67})_{0.9}O_{1.95}F_{0.05}$	10C/60 mAh g^{-1}	64%/100	[4]
$Na(Ni_{0.3}Fe_{0.2}Mn_{0.5})_{0.8}Ti_{0.1}Sb_{0.05}Co_{0.05}O_2$	5C/80 mAh g^{-1}	74.69%/300	[5]
$Na_{0.67}Ni_{0.33}Mn_{0.67}O_2$@MgO	2C/65 mAh g^{-1}	56%/200	[6]
$Na_{0.67}Ni_{0.33}Mn_{0.67}O_2$	2C/90 mAh g^{-1}	76.41%/200	[7]
O3-$Na_{0.95}CrO_2$	5C/40 mAh g^{-1}	80%/50	[8]
Na2/3Mn0.8Fe0.1Mg0.1O2	10C/60 mAh g^{-1}	86%/50	[9]
NaNi0.15Mn0.75O2	2C/70 mAh g^{-1}	82%/20	[10]
NaFe9/20Cr9/20Ti1/10O2	2C/60 mAh g^{-1}	70.6%/50	[11]

Table S7. The calculated band center values for the chosen atoms and projected orbitals in the range of (-8 eV ~ 4 eV).

		ε_d (eV)		ε_p (eV)		ε_s (eV)	
		up	down	up	down	up	down
NNM	Ni	-0.615	-1.854				
	Mn	-2.288	0.243				
	O			-3.295	-3.306		
NNM-S	Sr	-2.537	-2.121				
	Ni	-1.694	-1.075				
	Mn	-0.837	-0.456				
	O			-3.348	-3.279		
NNM-L	Li					-3.873	-3.729
	Ni	-1.512	-2.372				
	Mn	-1.967	-0.162				
	O			-3.301	-3.351		
NNM-LS	Li					-3.455	-3.174
	Ni	-1.107	-1.984				
	Mn	-1.932	-0.297				
	O			-3.331	-3.391		

[1] X. Li, J. Miao, W. Huang, K. Wang, H. Long, Y. Xu, Z. Wei, Y. Wu, M. Zhi, Z. Hong, The synergistic effect of Mg2+ and K+ in layered-oxide cathode materials for sodium-ion batteries, Electrochimica Acta 435 (2022) 141373. https://doi.org/https://doi.org/10.1016/j.electacta.2022.141373.

[2] C. Santamaría, E. Morales, C.d. Rio, B. Herradón, J.M. Amarilla, Studies on sodium-ion batteries: Searching for the proper combination of the cathode material, the electrolyte and the working voltage. The role of magnesium substitution in layered manganese-rich oxides, and pyrrolidinium ionic liquid, Electrochimica Acta 439 (2023) 141654. https://doi.org/https://doi.org/10.1016/j.electacta.2022.141654.

[3] C.-Y. Huang, S.K. Babu, W.-R. Liu, Temperature effects on P2 type-Na0.8Cu0.2Fe0.4Mn0.4O2 layer oxide cathode synthesized through a co-precipitation method for sodium ion batteries, Electrochimica Acta 543 (2025) 147541. https://doi.org/https://doi.org/10.1016/j.electacta.2025.147541.

[4] X. Chen, W. Guo, R. Li, P. Du, X. Zhan, S. Gao, Structure, Electrochemical, and Transport Properties of Li- and F-Modified P2-Na2/3Ni1/3Mn2/3O2 Cathode Materials for Na-Ion Batteries, Coatings 13(3) (2023) 626.

[5] W. Luo, W. Su, M. Hu, X. Wang, Enhancing rate and stability performance of O3-type NiFeMnTi-based layered oxides via Sb/Co dual-doping, Journal of Electroanalytical Chemistry 960 (2024) 118212. https://doi.org/https://doi.org/10.1016/j.jelechem.2024.118212.

[6] L. Xue, S. Bao, L. Yan, Y. Zhang, J. Lu, Y. Yin, MgO-Coated Layered Cathode

Oxide With Enhanced Stability for Sodium-Ion Batteries, Frontiers in Energy Research Volume 10 - 2022 (2022). https://doi.org/10.3389/fenrg.2022.847818.
[7] H. Deng, L. Liu, Z. Shi, Effect of copper substitution on the electrochemical properties of high entropy layered oxides cathode materials for sodium-ion batteries, Materials Letters 340 (2023) 134113. https://doi.org/https://doi.org/10.1016/j.matlet.2023.134113.
[8] K. Mathiyalagan, A. Ponnaiah, K. Karuppiah, S. Rengapillai, S. Marimuthu, Enhanced performance on layered O3-Na0.95CrO2 cathode material for emerging sodium-ion batteries, Ionics 26(8) (2020) 3929-3936. https://doi.org/10.1007/s11581-020-03523-7.
[9] Y. Li, Z.-Y. Li, K. Sun, Y.-T. Liu, D.-F. Chen, S.-B. Han, L.-F. He, M.-J. Li, X.-L. Liu, M.-M. Wu, Layered Co/Ni-free Mn-rich oxide P2-Na2/3Mn0.8Fe0.1Mg0.1O2 as high-performance cathode material for sodium-ion batteries, Ionics 26(2) (2020) 735-743. https://doi.org/10.1007/s11581-019-03208-w.
[10] V.H. Nguyen, L.T.N. Huynh, T.H. Nguyen, T.P. Vu, M.L.P. Le, A. Grag, V.M. Tran, Promising electrode material using Ni-doped layered manganese dioxide for sodium-ion batteries, Journal of Applied Electrochemistry 48(7) (2018) 793-800. https://doi.org/10.1007/s10800-018-1196-0.
[11] M. Kouthaman, P. Arjunan, K. Kannan, R. Subadevi, V. Kumaran, M. Sivakumar, Titanium deputized layered O3-type NaFe9/20Cr9/20Ti1/10O2 cathode material for sodium-ion batteries, Materials Letters 285 (2021) 129119. https://doi.org/https://doi.org/10.1016/j.matlet.2020.129119.